

Exceptional phase transition in a single Kerr-cat qubit

Pei-Rong Han¹, Tian-Le Yang^{2,3}, Wen Ning^{2,3}, Hao-Long

Zhang^{2,3}, Huifang Kang¹, Huiye Qiu^{1,*} and Zhen-Biao Yang^{2,3†}

¹*School of Physics and Mechanical and Electrical Engineering, Longyan University, Longyan 364012, China*

²*Fujian Key Laboratory of Quantum Information and Quantum Optics,*

College of Physics and Information Engineering,

Fuzhou University, Fuzhou, Fujian 350108, China

³*Department of Physics, Fuzhou University, Fuzhou 350108, China*

Exceptional points in non-Hermitian quantum systems give rise to novel genuine quantum phenomena. Recent explorations of exceptional-point-induced quantum phase transitions have extended from discrete-variable to continuous-variable-encoded quantum systems. However, quantum phase transitions driven by Liouvillian exceptional points (LEPs) in continuous-variable platforms remain largely unexplored. Here, we construct and investigate a Liouvillian exceptional structure based on a driven-dissipative Kerr-cat qubit. Through numerical simulations, we reveal a quantum phase transition occurring at the LEP characterized by a sudden change in dynamical behavior from underdamped oscillations to overdamped relaxations as visualized via Wigner functions and Bloch sphere trajectories. Notably the negativity of the Wigner function serves as a direct signature of genuine quantum coherence unattainable in conventional single-qubit non-Hermitian systems. Furthermore, we introduce the phase difference between the off-diagonal elements of the Liouvillian eigenmatrices as a novel parameter to quantify the transition. Our results establish the Kerr-cat qubit as a novel continuous-variable setting for exploring dissipative quantum criticality and intrinsic non-Hermitian physics.

Non-Hermitian physics has attracted considerable attention in recent years, with research advancing from classical [1–14] or semiclassical [15–30] regimes into the full quantum domain [31–45]. Recently, these studies have been extended from discrete-variable to continuous-variable quantum systems [46, 47]. These works explore distinct physical phenomena associated with Hamiltonian exceptional points (HEPs) and Liouvillian exceptional points (LEPs), such as entanglement phase transitions [46] and non-Hermitian topology [47]. An HEP is a singular point where both eigenvalues and eigenvectors of a non-Hermitian Hamiltonian coalesce; its experimental observation typically relies on post-selection [27–33]. In contrast, an LEP refers to the coalescence of eigenvalues and eigenvectors of a Liouvillian superoperator, which arises without post-selection and inherently incorporates all quantum jumps—a hallmark of genuinely open quantum dynamics [36–45]. While HEPs and LEPs share similar properties in the semiclassical limit, they exhibit fundamentally different behaviors in the quantum regime [35]. However, quantum phase transitions driven by LEPs in continuous-variable systems remain largely unexplored.

In this paper, we construct the Liouvillian superoperator for a continuous-variable system based on a single driven-dissipative Kerr-cat qubit [48–55]. Within this framework, the computational basis (Z-basis) is encoded using parity-symmetric cat states: the even-parity state $|\mathcal{C}_\alpha^+\rangle = \mathcal{N}_\alpha^+ (|\alpha\rangle + |-\alpha\rangle)$ and the odd-parity state

$|\mathcal{C}_\alpha^-\rangle = \mathcal{N}_\alpha^- (|\alpha\rangle - |-\alpha\rangle)$, where $|\pm\alpha\rangle$ are coherent states and $\mathcal{N}_\alpha^\pm = 1/\sqrt{2(1 \pm e^{-2|\alpha|^2})}$ are normalization constants. Accordingly, the X-basis states are defined as $|\pm X\rangle = |\pm\alpha\rangle$ and the Y-basis states as $|\pm Y\rangle = |\mathcal{C}_\alpha^{\mp i}\rangle = (|\mathcal{C}_\alpha^+\rangle \pm i|\mathcal{C}_\alpha^-\rangle)/\sqrt{2}$. This encoding leverages the degenerate eigenstate manifold of a Kerr-nonlinear resonator under two-photon driving, which provides a naturally noise-biased qubit subspace [48, 55, 56].

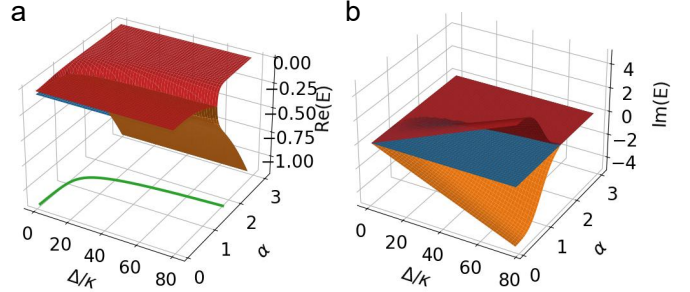


FIG. 1: Eigenspectrum of the Liouvillian matrix $\mathcal{L}_{\text{matrix}}$. Panels (a) and (b) depict the real and imaginary parts, respectively, with colors denoting different eigenvalues (excluding the steady-state eigenvalue $E_1 = 0$). The solid green curve in (a) indicates LEP2s in the Δ/α parameter space at fixed single-photon loss κ .

The non-Hermitian character of the system's Liouvillian originates from single-photon loss. This dissipation channel mediates bidirectional quantum jumps between the even- and odd-parity cat states, analogous to the jumps described by a σ_x operator in a conventional qubit. Introducing a detuning Δ between the two-photon drive frequency and the frequency of Kerr resonator lifts the degeneracy of the cat states, effectively implementing co-

*E-mail: qiuhiye@lyun.edu.cn

†E-mail: zbyang@fzu.edu.cn

herent rotations around the logical Z-axis of the qubit. By examining the evolution of the quantum state across different detunings, one can observe distinct dynamical behaviors in the vicinity of LEPs. Specifically, the system exhibits a phase transition induced by an LEP.

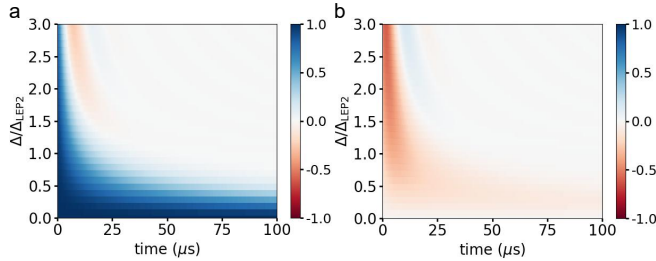


FIG. 2: Time evolution of (a) $\langle X \rangle$ and (b) $\langle Y \rangle$ under different detunings Δ . For $|\Delta| > \Delta_{\text{LEP2}}$, damped oscillations with exponential envelopes are observed. When $|\Delta| < \Delta_{\text{LEP2}}$, the system is overdamped without oscillation. At the critical point $|\Delta| = \Delta_{\text{LEP2}}$, critical damping occurs, leading to the fastest convergence to the steady state. The parameters are $\kappa/2\pi = 10$ kHz, $K/2\pi = 6.7$ MHz, $P/2\pi = 15.5$ MHz and $\kappa_\phi = 0$.

Our scheme is based on a Kerr-nonlinear resonator with a two-photon driving. In the rotating frame, the Hamiltonian for the system is given by (we set $\hbar \equiv 1$ throughout this paper)

$$H = \Delta a^\dagger a + K a^{\dagger 2} a^2 + P (a^{\dagger 2} + a^2), \quad (1)$$

where Δ is the driving-resonator detuning, K is the Kerr coefficient and P is the amplitude of the two-photon driving. $a^\dagger(a)$ is the creation (annihilation) operator for the Kerr-nonlinear resonator. When $\Delta = 0$, the Hamiltonian admits both coherent states $|\pm\alpha\rangle$ and cat states $|\mathcal{C}_\alpha^\pm\rangle$ as eigenstates for large α , where $\alpha = \sqrt{P/K}$. Throughout this paper, we assume K and P are positive and real, hence α is also real. These cat states

exhibit exact orthogonality $\langle \mathcal{C}_\alpha^k | \mathcal{C}_\alpha^j \rangle = \delta_{kj}$, while the coherent states are merely quasi-orthogonal for large α with $|\langle \alpha | -\alpha \rangle| = e^{-2\alpha^2}$. This coherent-state non-orthogonality modifies exceptional points within the cat-state encoding subspace, quantified by the ratio $p = \mathcal{N}_\alpha^+ / \mathcal{N}_\alpha^-$.

In experiments, systems inevitably interact with their environments through single-photon loss, described by the annihilation operator a with rate κ , and pure dephasing, described by the photon-number operator $a^\dagger a$ with rate κ_ϕ . The dynamics of this driven-dissipative system is governed by the Lindblad master equation

$$\dot{\rho} \equiv \mathcal{L}(\rho) = -i[H, \rho] + \sum_\mu \mathcal{D}[\mathcal{O}_\mu] \rho, \quad (2)$$

where \mathcal{L} is the Liouvillian superoperator, $\mathcal{D}[\mathcal{O}_\mu]$ are the dissipators associated with the jump operators \mathcal{O}_μ , $\mathcal{D}[\mathcal{O}_\mu]\rho = \mathcal{O}_\mu \rho \mathcal{O}_\mu^\dagger - \frac{1}{2} \mathcal{O}_\mu^\dagger \mathcal{O}_\mu \rho - \frac{1}{2} \rho \mathcal{O}_\mu^\dagger \mathcal{O}_\mu$ and ρ is the density matrix of the nonlinear resonator. The model described here fits within the topological classification framework for driven-dissipative systems, where steady-state structures and fluctuation dynamics are characterized by graph invariants [57, 58]. While single-photon loss ($\mathcal{O}_1 = \sqrt{\kappa}a$) typically introduces bit-flip errors that degrade the encoding subspace, it paradoxically drives the system toward steady states comprising statistical mixtures of parity-opposite cat states, $\rho_{ss} = p_1 |\mathcal{C}_\alpha^\pm\rangle \langle \mathcal{C}_\alpha^\pm| + p_2 |\mathcal{C}_\alpha^\mp\rangle \langle \mathcal{C}_\alpha^\mp|$ ($p_1 + p_2 \simeq 1$). In contrast, dephasing noise ($\mathcal{O}_2 = \sqrt{\kappa_\phi}a^\dagger a$) remains suppressed when the environmental noise bandwidth is narrower than the system's energy gap [52], yet still modifies the Liouvillian spectrum and dynamical behavior.

To study the Liouvillian spectra and LEPs, we use a vectorized representation to obtain the matrix form of the Liouvillian superoperator. Conditioned on the relations $a|\mathcal{C}_\alpha^\pm\rangle = \alpha p^{\pm 1} |\mathcal{C}_\alpha^\mp\rangle$ and $a^\dagger|\mathcal{C}_\alpha^\pm\rangle = \alpha p^{\mp 1} |\mathcal{C}_\alpha^\mp\rangle$, the matrix form of \mathcal{L} in the space spanned by $\{|\mathcal{C}_\alpha^+\rangle, |\mathcal{C}_\alpha^-\rangle\}$ can be expressed by a 4×4 matrix

$$\mathcal{L}_{\text{matrix}} = \begin{pmatrix} -\alpha^2 \kappa p^2 & 0 & 0 & \alpha^2 \kappa p^{-2} \\ 0 & \alpha^2 (-\frac{\kappa}{2} p_2^+ + i \Delta p_2^-) + L_\phi & \alpha^2 \kappa & -0 \\ 0 & \alpha^2 \kappa & \alpha^2 (-\frac{\kappa}{2} p_2^+ - i \Delta p_2^-) + L_\phi & 0 \\ \alpha^2 \kappa p^2 & -0 & 0 & -\alpha^2 \kappa p^{-2} \end{pmatrix}, \quad (3)$$

where $p_j^\pm = p^{-j} \pm p^j$ and $L_\phi = \kappa_\phi |\alpha|^4 (1 - p_4^+/2)$. Note that, for conventional qubits, LEPs can be designed independently of basis orthogonality. In our continuous-variable encoding, however, the parameter p indicates the overlap $\langle \alpha | -\alpha \rangle$. When $p \rightarrow 1$, this overlap vanishes, $\mathcal{L}_{\text{matrix}}$ reverts to a Hermitian form, precluding any exceptional point. This reveals a fundamental difference in how state overlap governs non-Hermitian physics.

The Liouvillian $\mathcal{L}_{\text{matrix}}$ yields four eigenvalues

$$E_1 = 0, \quad (4)$$

$$E_2 = -\kappa |\alpha|^2 p_2^+, \quad (5)$$

$$E_3 = \frac{E_2}{2} + L_\phi - i |\alpha|^2 \sqrt{(\Delta p_2^-)^2 - \kappa^2}, \quad (6)$$

$$E_4 = \frac{E_2}{2} + L_\phi + i |\alpha|^2 \sqrt{(\Delta p_2^-)^2 - \kappa^2}. \quad (7)$$

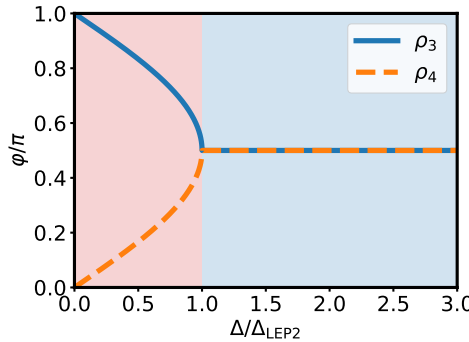


FIG. 3: The phase difference (φ) between the off-diagonal elements of ρ_3 (solid blue line) and ρ_4 (dashed orange line).

The eigenvalue E_1 corresponds to the steady state ρ_{ss} , while E_2 is strictly real and always associates with the eigenvector $\text{Vec}[\rho_2] = (-1, 0, 0, 1)^\top$. The remaining two eigenvalues, E_3 and E_4 , form a complex-conjugate pair, with eigenmatrices satisfying $\rho_3 = \rho_4^\dagger$. A second-order exceptional point (LEP2) occurs when the detuning reaches $|\Delta| = \Delta_{\text{LEP2}} \equiv \kappa/p_2^-$. At this critical point, E_3 and E_4 coalesce into a single eigenvalue $E_2/2$ with $\kappa_\phi = 0$, and their eigenvectors merge into $\text{Vec}[\rho_{\text{EP}}] = (0, i, 1, 0)^\top$. This spectral structure is illustrated in Fig. 1 for the parameters $\kappa/2\pi = 10$ kHz and $\kappa_\phi = 0$, where the solid green curve demonstrates the exponential scaling of Δ_{LEP2} with the cat-state amplitude α .

Accordingly, when $\kappa_\phi \neq 0$, the Liouvillian eigenvalues E_1 and E_2 remain unchanged, while E_3 and E_4 exhibit shifts in their real parts by L_ϕ . Remarkably, the parameters of LEPs remain unchanged. This result demonstrates that dephasing modifies exclusively the imaginary components of the corresponding non-Hermitian Hamiltonian spectrum, altering dissipation rates while preserving coherent oscillations—consistent with the phase-noise resilience mechanism for cat states [55].

As shown in Fig. 1, for a fixed value of α , the LEP2 separates the Liouvillian spectrum into two distinct regimes. For $|\Delta| < \Delta_{\text{LEP2}}$, all eigenvalues are purely real, whereas a complex spectrum emerges for $|\Delta| > \Delta_{\text{LEP2}}$. The imaginary parts of the eigenvalues set the oscillation periods of the dynamical evolution, while the real parts govern the decay rates. Therefore, the phase transition at the LEP2 can be directly observed from the distinctive dynamical behavior of the state evolution. The system's dynamical evolution is governed by

$$\rho(t) = c_1 \exp(E_1 t) \rho_{ss} + \sum_{i=2}^4 c_i \exp(E_i t) \rho_i, \quad (8)$$

where c_i denote expansion coefficients, E_i are the eigenvalues, and ρ_i are the corresponding eigenvectors of $\mathcal{L}_{\text{matrix}}$. Crucially, when $|\Delta| < \Delta_{\text{LEP2}}$, the time evolution of $c_i \exp(E_i t)$ manifests exponential behavior due to the absence of imaginary components in E_i , while for $|\Delta| > \Delta_{\text{LEP2}}$, these coefficients display exponentially

damped periodic oscillations arising from complex eigenvalue pairs. This dynamical dichotomy defines two distinct phases separated by LEP2s. The system relaxes to its steady state in the long-time limit.

To observe this phase transition, we initialize the system in the coherent state $|\alpha\rangle$ and apply the two-photon drive with variable duration across different detunings Δ . The simulation parameters are set to $K/2\pi = 6.7$ MHz, $P/2\pi = 15.5$ MHz, and $\kappa/2\pi = 10$ kHz, as reported in Ref. [48]. From K and P , the cat-state amplitude follows as $\alpha = \sqrt{P/K} \approx 1.52$. As demonstrated in Fig. 2, two contrasting dynamical regimes emerge. For detunings exceeding Δ_{LEP2} , damped oscillations in $\langle X \rangle \langle Y \rangle$ signal underdamped dynamics, whereas for $|\Delta| < \Delta_{\text{LEP2}}$, $\langle X \rangle \langle Y \rangle$ undergoes monotonic exponential decay characteristic of overdamped behavior. This abrupt transition at $|\Delta| = \Delta_{\text{LEP2}}$ stems directly from Liouvillian eigenvalues and eigenvectors coalescence.

This exceptional phase transition can be further quantified by the phase difference φ between the off-diagonal elements of the eigenmatrices ρ_3 or ρ_4 . For an eigenmatrix ρ_j (with $j = 3, 4$) expressed in the cat-state basis $\{|\mathcal{C}_\alpha^+\rangle, |\mathcal{C}_\alpha^-\rangle\}$ as

$$\rho_j = \begin{pmatrix} \rho_{00} & \rho_{01} \\ \rho_{10} & \rho_{11} \end{pmatrix}, \quad (9)$$

the phase difference φ is defined as

$$\varphi \equiv |\arg(\rho_{01}) - \arg(\rho_{10})|, \quad (10)$$

where $\arg(\cdot)$ denotes the complex argument. As shown in Fig. 3, the variation of φ with Δ provides a clear signature of the phase transition across the LEP. In contrast to previous study that characterized the phase difference between eigenstates of a non-Hermitian Hamiltonian [31], our work focuses on the phase difference associated with the eigenvectors of the Liouvillian superoperator—a distinct aspect that has not been addressed before.

The dynamical dichotomy is further resolved through phase-space visualization. The quantum state ρ is fully characterized by its Wigner function

$$W(\beta) = \frac{2}{\pi} \text{Tr} [D(-\beta) \rho D(\beta) e^{i\pi a^\dagger a}], \quad (11)$$

with $D(\beta)$ denoting the displacement operator. This phase-space representation provides complete information about the oscillator's quantum state. When $|\Delta| > \Delta_{\text{LEP2}}$, quantum-state oscillations between $|\alpha\rangle$ and $|\alpha\rangle$ periodically generate coherent interference fringes in the Wigner function (Fig. 4c), reflecting non-classical coherence before convergence to ρ_{ss} . In contrast, for $|\Delta| < \Delta_{\text{LEP2}}$, the Wigner function shows direct relaxation to ρ_{ss} without oscillatory features (Fig. 4d). Complementary insights emerge from Bloch sphere trajectories in Fig. 4a,b. The underdamped regime exhibits repeated crossings of the YZ-plane, where a larger detuning Δ yields more frequent crossings, signifying $\langle X \rangle$ oscillations. In contrast, the overdamped regime displays

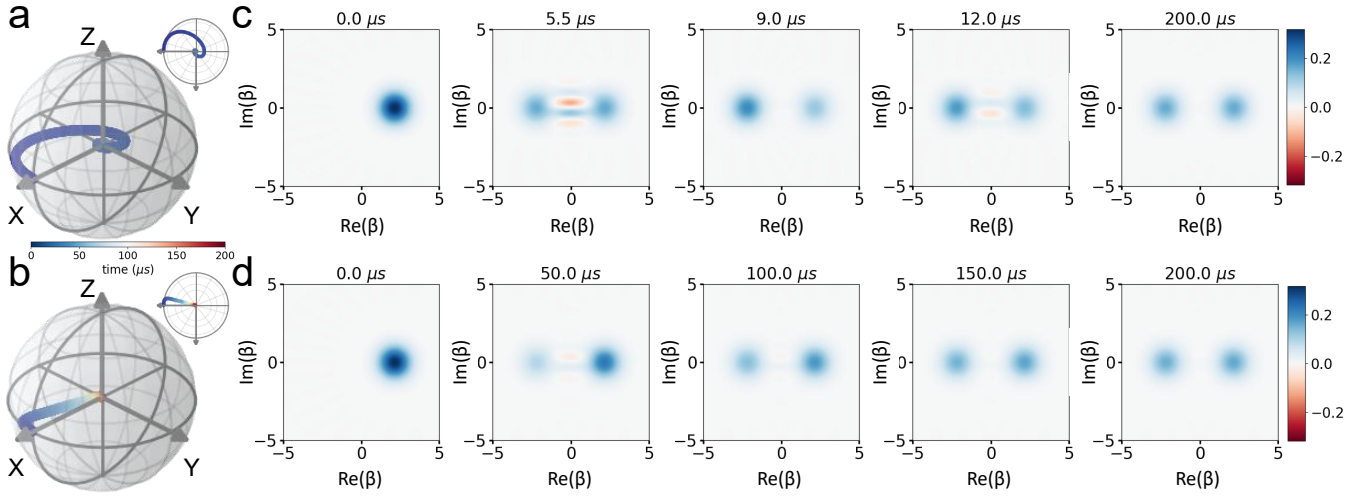


FIG. 4: Bloch representation of quantum state evolution and the corresponding Wigner functions. Evolution trajectories for (a) $|\Delta| = 3\Delta_{\text{LEP2}}$ and (b) $|\Delta| = 0.5\Delta_{\text{LEP2}}$. All trajectories are confined to the XY-plane. The inset at the upper right shows a top-down view of the trajectory, with its color corresponding to the evolution time. (a) For $|\Delta| > \Delta_{\text{LEP2}}$, the trajectory spirals inward toward the origin (steady state). (b) For $|\Delta| < \Delta_{\text{LEP2}}$, the trajectory converges monotonically toward the origin without spiraling. Panels (c) and (d) show the corresponding Wigner functions at different evolution times. (c) When $|\Delta| > \Delta_{\text{LEP2}}$, interference fringes periodically emerge and vanish before reaching steady state. (d) When $|\Delta| < \Delta_{\text{LEP2}}$, interference fringes appear only transiently before each steady state is achieved. The parameters are $\kappa/2\pi = 10$ kHz, $K/2\pi = 6.7$ MHz, $P/2\pi = 15.5$ MHz and $\kappa_\phi = 0$.

radial convergence to the origin without equatorial intersections, confirming the absence of $\langle X \rangle$ switching.

To quantify how well the system remains confined to the Kerr-cat qubit subspace during evolution, we compare the state $\sigma(t)$ obtained from the effective Liouvillian dynamics of Eq. (8) with the state $\rho(t)$ obtained from the full master equation of Eq. (2). Their closeness is measured by the Uhlmann fidelity $F(\rho, \sigma) = (\text{Tr} \sqrt{\sqrt{\rho} \sigma \sqrt{\rho}})^2$. Figure 5 displays the fidelity as a function of detuning and time for the initial state $|\alpha\rangle$. Over the selected parameter range, the two evolutions show excellent agreement. Furthermore, as the system relaxes toward its steady state, the fidelity asymptotically approaches unity. The minor deviations stem from the detuning term $\Delta a^\dagger a$, which is not fully captured in the effective Liouvillian description. This term lifts the cat-state degeneracy due to their different photon numbers ($\alpha^2 p^2$ vs. α^2 / p^2), and can induce leakage out of the encoded subspace.

In summary, we have revealed and characterized a quantum phase transition directly induced by an LEP2 in a single driven-dissipative Kerr-cat qubit. Through analysis of the Liouvillian spectrum and dynamics, we have demonstrated that the transition is marked by a sharp change in dynamical behavior from underdamped oscillations to overdamped relaxations as the detuning crosses the exceptional point. Furthermore, the phase difference between off-diagonal elements of the Liouvillian eigenmatrices emerges as a distinct and previously unreported signature of this exceptional transition. The negativity of the Wigner function serves as a direct hallmark of genuine quantum coherence, a feature unattainable in conventional single-qubit non-Hermitian systems.

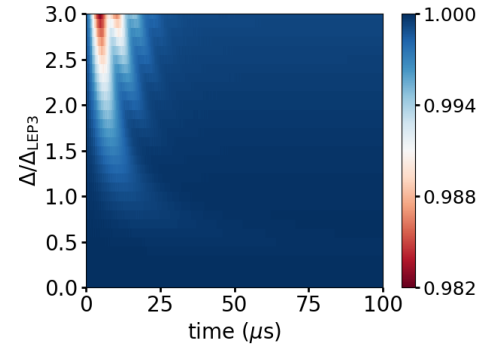


FIG. 5: Validation of the Liouvillian dynamics. Color represents the fidelity $F(\rho_H, \rho_L)$ between states evolved under the Lindblad master equation of Eq. (2) and the Liouvillian approximation of Eq. (8). Here, we set $K/2\pi = 6.7$ MHz, $P/2\pi = 15.5$ MHz, $\kappa/2\pi = 10$ kHz, and $\kappa_\phi = 0$.

Our results establish the Kerr-cat qubit as a versatile platform for exploring dissipative quantum criticality and intrinsic non-Hermitian physics, thereby bridging fault-tolerant bosonic encoding with the study of open quantum phase transitions.

This work was supported by the National Natural Science Foundation of China (Grant Nos. 12505021, 12475015, 12505016), the Natural Science Foundation of Fujian Province (Grant Nos. 2025J01383, 2025J01465) and the Research Startup Funds of Longyan University (LB2025002).

[1] C. Dembowski, H.-D. Gräf, H. L. Harney, A. Heine, W. D. Heiss, H. Rehfeld, and A. Richter, Experimental observation of the topological structure of exceptional points, *Phys. Rev. Lett.* **86**, 787 (2001).

[2] Y. Choi, S. Kang, S. Lim, W. Kim, J.-R. Kim, J.-H. Lee, and K. An, Quasieigenstate coalescence in an atom-cavity quantum composite, *Phys. Rev. Lett.* **104**, 153601 (2010).

[3] T. Gao et al., Observation of non-Hermitian degeneracies in a chaotic exciton-polariton billiard, *Nature (London)* **526**, 554 (2015).

[4] D. Zhang, X.-Q. Luo, Y.-P. Wang, T.-F. Li, and J.Q. You, Observation of the exceptional point in cavity magnon polaritons, *Nat. Commun.* **8**, 1368 (2017).

[5] F. E. Öztürk, T. Lappe, G. Hellmann, J. Schmitt, J. Klaers, and F. Vewinger, Observation of a non-Hermitian phase transition in an optical quantum gas, *Science* **372**, 88 (2021).

[6] W. Tang, X. Jiang, K. Ding, Y.-X. Xiao, Z.-Q. Zhang, C.T. Chan, and G. Ma, Exceptional nexus with a hybrid topological invariant, *Science* **370**, 1077 (2020).

[7] K. Wang, A. Dutt, K.Y. Yang, C.C. Wojcik, J. Vukovi, and S. Fan, Generating arbitrary topological windings of a non-Hermitian band, *Science* **371**, 1240 (2021).

[8] K. Wang, A. Dutt, C. C. Wojcik, and S. Fan, Topological complex-energy braiding of non-Hermitian bands, *Nature (London)* **598**, 59 (2021).

[9] Y. S. S. Patil, J. Höller, P. A. Henry, C. Guria, Y. Zhang, L. Jiang, N. Kralj, N. Read, and J. G. E. Harris, Measuring the knot of non-Hermitian degeneracies and non-commuting braids, *Nature (London)* **607**, 271 (2022).

[10] J. Doppler, A. A. Mailybaev, J. Böhm, U. Kuhl, A. Girschik, F. Libisch, T. J. Milburn, P. Rabl, N. Moiseyev, and S. Rotter, Dynamically encircling an exceptional point for asymmetric mode switching, *Nature (London)* **537**, 76 (2016).

[11] H. Xu, D. Mason, L. Jiang, and J. G. E. Harris, Topological energy transfer in an optomechanical system with exceptional points, *Nature (London)* **537**, 80 (2016).

[12] J. W. Yoon et al., Time-asymmetric loop around an exceptional point over the full optical communication band, *Nature (London)* **562**, 86 (2018).

[13] W. Chen, S.K. Özdemir, G. Zhao, J. Wiersig, and L. Yang, Exceptional points enhance sensing in an optical micro cavity, *Nature (London)* **548**, 192 (2017).

[14] H. Hodaei, A.U. Hassan, S. Wittek, H. Garcia-Gracia, R. El-Ganainy, D. N. Christodoulides, and M. Khajavikhan, Enhanced sensitivity at higher-order exceptional points, *Nature (London)* **548**, 187 (2017).

[15] S. Yu et al., Experimental investigation of quantum PT enhanced sensor, *Phys. Rev. Lett.* **125**, 240506 (2020).

[16] K. Wang, L. Xiao, J. C. Budich, W. Yi, and P. Xue, Simulating exceptional non-Hermitian metals with single-photon interferometry, *Phys. Rev. Lett.* **127**, 026404 (2021).

[17] Y.-L. Fang, J.-L. Zhao, Y. Zhang, D.-X. Chen, Q.-C. Wu, Y.-H. Zhou, C.-P. Yang, and F. Nori, Experimental demonstration of coherence flow in PT- and anti-PT-symmetric systems, *Commun. Phys.* **4**, 223 (2021).

[18] P. Peng, W. Cao, C. Shen, W. Qu, J. Wen, L. Jiang, and Y. Xiao, Anti-parity-time symmetry with flying atoms, *Nat. Phys.* **12**, 1139 (2016).

[19] J. Li, A. K. Harter, J. Liu, L. d. Melo, Y. N. Joglekar, and L. Luo, Observation of parity-time symmetry breaking transitions in a dissipative Floquet system of ultracold atoms, *Nat. Commun.* **10**, 855 (2019).

[20] Z. Ren, D. Liu, E. Zhao, C. He, K. K. Pak, J. Li, and G.-B. Jo, Chiral control of quantum states in non-Hermitian spin-orbit-coupled fermions, *Nat. Phys.* **18**, 385 (2022).

[21] W.-C. Wang et al., Observation of \mathcal{PT} -symmetric quantum coherence in a single-ion system, *Phys. Rev. A* **103**, L020201 (2021).

[22] L. Ding, K. Shi, Q. Zhang, D. Shen, X. Zhang, and W. Zhang, Experimental determination of \mathcal{PT} -symmetric exceptional points in a single trapped ion, *Phys. Rev. Lett.* **126**, 083604 (2021).

[23] Y. Wu, W. Liu, J. Geng, X. Song, X. Ye, C. K. Duan, X. Rong, and J. F. Du, Observation of parity-time symmetry breaking in a single-spin system, *Science* **364**, 878 (2019).

[24] W. Liu, Y. Wu, C.-K. Duan, X. Rong, and J. Du, Dynamically encircling an exceptional point in a real quantum system, *Phys. Rev. Lett.* **126**, 170506 (2021).

[25] W. Zhang, X. Ouyang, X. Huang, X. Wang, H. Zhang, Y. Yu, X. Chang, Y. Liu, D.-L. Deng, and L.-M. Duan, Observation of non-Hermitian topology with nonunitary dynamics of solid-state spins, *Phys. Rev. Lett.* **127**, 090501 (2021).

[26] S. Dogra, A. A. Melnikov, and G. S. Paraoanu, Quantum simulation of parity-time symmetry breaking with a superconducting quantum processor, *Commun. Phys.* **4**, 26 (2021).

[27] M. Naghiloo, M. Abbasi, Y. N. Joglekar, and K. W. Murch, Quantum state tomography across the exceptional point in a single dissipative qubit, *Nat. Phys.* **15**, 1232 (2019).

[28] Z. Wang, Z. Xiang, T. Liu, X. Song, P. Song, X. Guo, L. Su, H. Zhang, Y. Du, and D. Zheng, Observation of the exceptional point in superconducting qubit with dissipation controlled by parametric modulation, *Chin. Phys. B* **30**, 100309 (2021).

[29] M. Naghiloo, M. Abbasi, Y. N. Joglekar, and K. W. Murch, Quantum state tomography across the exceptional point in a single dissipative qubit, *Nat. Phys.* **15**, 1232 (2019).

[30] M. Abbasi, W. Chen, M. Naghiloo, Y. N. Joglekar, K. W. Murch, Topological Quantum State Control through Exceptional-Point Proximity, *Phys. Rev. Lett.* **128**, 160401 (2022).

[31] P. R. Han, F. Wu, X. J. Huang, H. Z. Wu, C. L. Zou, W. Yi, M. Zhang, H. Li, K. Xu, D. Zheng, H. Fan, J. Wen, Z. B. Yang, and S. B. Zheng, Exceptional entanglement phenomena: Non-Hermiticity meeting non-classicality, *Phys. Rev. Lett.* **131**, 260201 (2023).

[32] P.-R. Han, W. Ning, X.-J. Huang, R.-H. Zheng, S.-B. Yang, F. Wu, Z.-B. Yang, Q.-P. Su, C.-P. Yang, and S.-B. Zheng, Measuring topological invariants for higher-order exceptional points in quantum three-mode systems, *Nat. Commun.* **15**, 10293 (2024).

[33] H.-L. Zhang, P.-R. Han, X.-J. Yu, S.-B. Yang, J.-H. Lü, W. Ning, C.-P. Yang, Z.-B. Yang, Q.-P. Su, and S.-B. Zheng, Implementation and topological characterization

of Weyl exceptional rings in quantum-mechanical systems, *Sci. Bull.* **70**, 2446 (2025).

[34] H.-L. Zhang, P.-R. Han, F. Wu, W. Ning, Z.-B. Yang, and S.-B. Zheng, Experimental Observation of Non-Markovian Quantum Exceptional Points, *Phys. Rev. Lett.* **135**, 230203 (2025).

[35] F. Minganti, A. Miranowicz, R. W. Chhajlany, and F. Nori, Quantum exceptional points of non-Hermitian Hamiltonians and Liouvillians: The effects of quantum jumps, *Phys. Rev. A* **100**, 062131 (2019).

[36] I. I. Arkhipov, A. Miranowicz, F. Minganti, and F. Nori, Quantum and semiclassical exceptional points of a linear system of coupled cavities with losses and gain within the Scully-Lamb laser theory, *Phys. Rev. A* **101**, 013812 (2020).

[37] F. Minganti, A. Miranowicz, R. W. Chhajlany, I. I. Arkhipov, and F. Nori, Hybrid-liouvillian formalism connecting exceptional points of non hermitian hamiltonians and liouvillians via postselection of quantum trajectories, *Phys. Rev. A* **101**, 062112 (2020).

[38] I. I. Arkhipov, A. Miranowicz, F. Minganti, and F. Nori, Liouvillian exceptional points of any order in dissipative linear bosonic systems: Coherence functions and switching between \mathcal{PT} and anti- \mathcal{PT} symmetries, *Phys. Rev. A* **102**, 033715 (2020).

[39] S. Khandelwal, N. Brunner, and G. Haack, Signatures of Liouvillian Exceptional Points in a Quantum Thermal Machine, *PRX Quantum* **2**, 040346 (2021).

[40] K. Sun, and W. Yi, Encircling the Liouvillian exceptional points: a brief review, *AAPPS Bull.* **34**, 22 (2024).

[41] W. Chen, M. Abbasi, Y. N. Joglekar, and K. W. Murch, Quantum Jumps in the Non-Hermitian Dynamics of a Superconducting Qubit, *Phys. Rev. Lett.* **127**, 140504 (2021).

[42] W. Chen, M. Abbasi, B. Ha, S. Erdamar, Y. N. Joglekar, and K. W. Murch, Decoherence-Induced Exceptional Points in a Dissipative Superconducting Qubit, *Phys. Rev. Lett.* **128**, 110402 (2022).

[43] S. Abo, P. Tulewicz, K. Bartkiewicz, S. K. Özdemir, and A. Miranowicz, Experimental Liouvillian exceptional points in a quantum system without Hamiltonian singularities, *New J. Phys.* **26**, 123032 (2024).

[44] J.-W. Zhang, J.-Q. Zhang, G.-Y. Ding, J.-C. Li, J.-T. Bu, B. Wang, L.-L. Yan, S.-L. Su, L. Chen, F. Nori, S. K. Özdemir, F. Zhou, H. Jing, and M. Feng, Dynamical control of quantum heat engines using exceptional points, *Nat. Commun.* **13**, 6225 (2022).

[45] J.-T. Bu, J.-Q. Zhang, G.-Y. Ding, J.-C. Li, J.-W. Zhang, B. Wang, W.-Q. Ding, W.-F. Yuan, L. Chen, S. K. Özdemir, F. Zhou, H. Jing, and M. Feng, Enhancement of Quantum Heat Engine by Encircling a Liouvillian Exceptional Point, *Phys. Rev. Lett.* **130**, 110402 (2023).

[46] K.-X. Yan, Z.C. Shi, Y.H. Chen, and Y. Xia, Controllable Non-Hermitianity in Continuous-Variable Qubits, <https://arxiv.org/abs/2511.04110v1>.

[47] P.-R. Han, H. Qiu, H.-L. Zhang, W. Ning, Z.-B. Yang, and S.-B. Zheng, Non-Hermitian topology in a single driven-dissipative Kerr-Cat qubit, <https://doi.org/10.48550/arXiv.2511.18482>.

[48] A. Grimm, N. E. Frattini, S. Puri, S. O. Mundhada, S. Touzard, M. Mirrahimi, S. M. Girvin, S. Shankar, M. H. Devoret, Stabilization and operation of a Kerr-cat qubit, *Nature* **584**, 205 (2020).

[49] Z. Leghtas, S. Touzard, I. M. Pop, A. Kou, B. Vlastakis, A. Petrenko, K. M. Sliwa, A. Narla, S. Shankar, M. J. Hatridge, M. Reagor, L. Frunzio, R. J. Schoelkopf, M. Mirrahimi, M. H. Devoret, Confining the state of light to a quantum manifold by engineered two-photon loss, *Science* **347**, 853 (2015).

[50] S. Puri, S. Boutin, A. Blais, Engineering the quantum states of light in a Kerr-nonlinear resonator by two-photon driving, *npj Quantum Inf.* **3**, 18 (2017).

[51] B. Vlastakis, G. Kirchmair, Z. Leghtas, S. E. Nigg, L. Frunzio, S. M. Girvin, M. Mirrahimi, M. H. Devoret, R. J. Schoelkopf, Deterministically Encoding Quantum Information Using 100-Photon Schrödinger Cat States, *Science* **342**, 607 (2013).

[52] S. Puri, A. Grimm, P. Campagne-Ibarcq, A. Eickbusch, K. Noh, G. Roberts, L. Jiang, M. Mirrahimi, M. H. Devoret, S. M. Girvin, Stabilized Cat in a Driven Nonlinear Cavity: A Fault-Tolerant Error Syndrome Detector, *Phys. Rev. X* **9**, 041009 (2019).

[53] H. Goto, Universal quantum computation with a nonlinear oscillator network, *Phys. Rev. A* **93**, 050301 (2016).

[54] F. Minganti, N. Bartolo, J. Lolli, W. Casteels, C. Ciuti, Exact results for Schrödinger cats in driven-dissipative systems and their feedback control, *Sci. Rep.* **6**, 26987 (2016).

[55] M. Mirrahimi, Z. Leghtas, V. V. Albert, S. Touzard, R. J. Schoelkopf, L. Jiang, M. H. Devoret, Dynamically protected cat-qubits: a new paradigm for universal quantum computation, *New J. Phys.* **16**, 045014 (2014).

[56] R. Lescanne, M. Villiers, T. Peronnin, A. Sarlette, M. Delbecq, B. Huard, T. Kontos, M. Mirrahimi, and Z. Leghtas, Exponential suppression of bit-flips in a qubit encoded in an oscillator, *Nat. Phys.* **16**, 509 (2020).

[57] G. Villa1, J. del Pino1, V. Dumont, G. Rastelli, M. Michalek, A. Eichler, and O. Zilberberg, Topological classification of driven-dissipative nonlinear systems, *Sci. Adv.* **11**, eadtk9311 (2025).

[58] K. Seibold, G. Villa, J. del Pino, and O. Zilberberg, Manifestations of flow topology in a quantum driven-dissipative system, <https://arxiv.org/abs/2508.16486v1>.